The effect of large-scale spectral forcing schemes on scale-dependent anisotropy in homogeneous turbulence

D. VALLEFUOCO[a], F. S. GODEFERD, A. NASO

Laboratoire de Mécanique des Fluides et d'Acoustique, UMR 5509 CNRS,
École centrale de Lyon, Université de Lyon, INSA de Lyon
a. donato.vallefuoco@ec-lyon.fr

Résumé :

Nous présentons des simulations numériques directes de turbulence homogène qui ont pour but d'étudier les effets de schémas de forçage à grande échelle sur l'anisotropie aux différentes échelles du champ de vitesse. Cette anisotropie est caractérisée au moyen de spectres dépendant de l'orientation du vecteur d'onde, pour l'énergie, l'hélicité, et la polarisation. Deux types de forçages sont étudiés : le forçage ABC basé sur un seul nombre d'onde, et le forçage dynamique de type "équations d'Euler" aux nombres d'onde infrarouges. Nous sommes ainsi en mesure de caractériser précisément les conditions de création de l'anisotropie dans les échelles inertielles de la turbulence.

Abstract :

We performed DNS of homogeneous turbulence in order to investigate the effect of large-scale spectral forcing schemes on the velocity field scale-dependent anisotropy, characterized by the measurement of angle-dependent energy, helicity and polarization spectra. Two kinds of forcing are considered: the ABC single wavenumber scheme, and the dynamical Euler infrared-range scheme. The conditions that allow anisotropy to develop in inertial scales were identified.

Keywords : DNS; isotropic turbulence; large-scale spectral forcing; scale-dependent anisotropy; angle-dependent spectra

1 Introduction

According to the classical K41 theory, in turbulent flows at asymptotically large Reynolds number, the large-scale dynamics should affect small scales statistical properties only through the energy production rate, *i.e.* small scales are statistically independent of large scales and have a universal behaviour. This assumption, referred to as the local isotropy hypothesis, has been studied by many authors but may be debated in actual implementations of turbulent flows, experimental or numerical. In particular Yeung & Brasseur (1991) [5] observed small scale anisotropy in numerical simulations with anisotropic large-scale forcing, and on the base of a small/large scale triadic interactions analysis it was argued that local

anisotropy persists at asymptotically high Reynolds number. It is therefore clear that energy and helicity production mechanisms can strongly influence the features of the produced turbulent field, and even affect the dynamics of inertial and small scales.

In order to study statistically stationary turbulence, many velocity forcing schemes have been used in numerical simulations so far. In particular, large-scale spectral forcing methods were used in homogeneous spectral simulations and consist in providing energy to the low wavenumber modes, which is consistent with the concept of Richardson cascade, see *e.g.* [3], [7], [10]. However in large-scale spectral forced simulations, anisotropy may develop because of the intrinsic anisotropy of the Fourier representation of velocity in a periodic box (only a finite number of discretized wavenumbers in a given spherical shell). Detection of this kind of anisotropy requires angle-dependent statistics. The motivation of this present study comes for instance from previous studies of freely decaying rotating turbulence, in which a refined anisotropic characterization was absolutely required to understand the subtle effect of the Coriolis force on each scale of the flow (see *e.g.* [16] or [14]). However, the drop in Reynolds number was severe due to dissipation, so that forced rotating turbulence should be considered. The following question is therefore pregnant: what would be the respective anisotropic "trace" of the forcing with respect to "natural" anisotropy creation due to rotation? This is why in this paper we analyze two forcing schemes representative of large-scale forcing, the Euler and the ABC forcing methods [8, 13], through this kind of anisotropy indicators. In particular the impact of these two forcing methods on the produced turbulence scale-dependent anisotropy will be characterized by energy, helicity and polarization angular spectra. We will first describe the Euler and the ABC forcing schemes in section 2, then in section 3 we will compare them and show how the development of anisotropy depends on the forcing input parameters. Finally in section 4 we will identify the conditions that allow anisotropy to develop in inertial ranges.

2 Forcing schemes

The goal of forcing turbulence is to represent, as a model force, the essential features of forcing mechanisms in more complex turbulent flows. For instance, the well-known Von Karman experiment consists of two counter rotating rotors, that not only inject momentum at large scales in the flow, but also involve a helicity contribution. In other contexts, for instance in geophysical flows, one would like to model the effect of a large scale instability that injects energy in the flow and trigger an energy cascade at smaller scales. For this reason, we wish to investigate the possibility of representing these mechanisms through simple models —here, the Euler and ABC forcing schemes— and to study their impact on the anisotropy of the flow, including the possibility of injection of helicity.

Helicity density is the scalar product between velocity and vorticity, $\mathcal{H} = \boldsymbol{u} \cdot \boldsymbol{\omega}$, and its integral is an ideal invariant [1, 6]. Since $\mathcal{H}$ is a pseudoscalar quantity, any turbulent flow with non-vanishing mean helicity $< \mathcal{H} >$ lacks mirror-symmetry. The wavenumber-dependent helicity spectrum is

$$H(k) = \int \hat{\boldsymbol{\omega}} \cdot \hat{\boldsymbol{u}}^* \, \delta(|\boldsymbol{k}| - k) \, \mathrm{d}\boldsymbol{k} \tag{1}$$

By the Schwarz inequality one can find

$$|h(\boldsymbol{k})| \leq 2 \, |\boldsymbol{k}| \, e(\boldsymbol{k}) \tag{2}$$

where $h(\boldsymbol{k}) = \hat{\boldsymbol{\omega}}(\boldsymbol{k}) \cdot \hat{\boldsymbol{u}}^*(\boldsymbol{k})$ is the helicity associated with a wavevector $\boldsymbol{k}$, and $e(\boldsymbol{k}) = \frac{1}{2} \, \hat{\boldsymbol{u}}(\boldsymbol{k}) \cdot \hat{\boldsymbol{u}}(\boldsymbol{k})^*$

is the kinetic energy density associated with $\boldsymbol{k}$. Relative helicity can be defined as

$$\mathcal{H}_{\text{rel}} = \frac{< \mathcal{H} > L_h}{K} \tag{3}$$

where $K = \iiint e(\boldsymbol{k})\,\mathrm{d}\boldsymbol{k}$ is the total turbulent kinetic energy and L_h is the integral length scale, defined from the spherically integrated kinetic energy spectrum $E(k) = \iint_{S(k)} e(\boldsymbol{k})\,\mathrm{d}\boldsymbol{k}$ ($S(k)$ is the sphere with radius k) as

$$L_h = \frac{1}{2}\frac{\int_0^{k_{\max}} E(k)\,\mathrm{d}k}{\int_0^{k_{\max}} k\,E(k)\,\mathrm{d}k} \tag{4}$$

From the Schwarz inequality (2), $\mathcal{H}_{\text{rel}} \leq 1$.

Another quantity that will be used in section 3 for characterizing the flow anisotropy is the polarization, which can be easily defined as a function of the Fourier coefficients components in the Craya-Herring frame of reference. The Craya-Herring frame is a frame of reference in Fourier space that allows to express a solenoidal field through only two components in the plane normal to the wavenumber (see *e.g.* [12])

$$\hat{\boldsymbol{u}}(\boldsymbol{k}) = u^{(1)}(\boldsymbol{k})\boldsymbol{e}^{(1)}(\boldsymbol{k}) + u^{(2)}(\boldsymbol{k})\boldsymbol{e}^{(2)}(\boldsymbol{k}) \tag{5}$$

once an a priori base "vertical" direction $\boldsymbol{n}$ is chosen to define

$$\boldsymbol{e}^{(1)} = \frac{\boldsymbol{k}\times\boldsymbol{n}}{|\boldsymbol{k}\times\boldsymbol{n}|}, \quad \boldsymbol{e}^{(2)} = \boldsymbol{e}^{(3)}\times\boldsymbol{e}^{(1)}, \quad \boldsymbol{e}^{(3)} = \frac{\boldsymbol{k}}{k}. \tag{6}$$

The decomposition (5) is particularly adapted to examine flows statistically axisymmetric about $\boldsymbol{n}$, but can still be used as a first step towards characterizing anisotropy of turbulence through angle-dependent statistics, the angle being the polar angle θ of $\boldsymbol{k}$ about $\boldsymbol{n}$. If $|\boldsymbol{k}\times\boldsymbol{n}| \neq 0$, $\boldsymbol{e}^{(1)}$ and $\boldsymbol{e}^{(2)}$ are directed respectively along parallels and meridians of spheres of radius $|\boldsymbol{k}|$ and $u^{(1)}$ and $u^{(2)}$ are the *toroidal* and the *poloidal* components. The polarization is defined as (see [12] for details)

$$\boldsymbol{Z}(\boldsymbol{k}) = \frac{1}{2}(< u^{(2)*}u^{(2)} > - < u^{(1)*}u^{(1)} > + i\Re < u^{(1)*}u^{(2)} >). \tag{7}$$

$\boldsymbol{Z}(\boldsymbol{k})$ quantifies the difference and correlation between toroidal and poloidal velocity components, as a refined tool for characterizing the anisotropy of turbulent statistics in spectral space. In the coming figures of section 3, the difference between E_{pol} and E_{tor}, the respective spectra of the toroidal and poloidal components (the real part of Z), is normalized by the energy spectrum.

We performed DNS with two different large-scale spectral forcing schemes: Euler forcing and ABC forcing (see *e.g.* [8] and [13]). In Euler-forced simulations, the lowest modes ($0 \leq |\boldsymbol{k}| \leq k_F$, where k_F is the maximum forcing wavenumber) obey the three-dimensional incompressible Euler equations and are independent of the other modes ($|\boldsymbol{k}| > k_F$) which are solutions of the incompressible Navier-Stokes equations. Some important physical and mathematical problems related to the Euler equations are still open, but the study of these problems is beyond the aim of this paper. The nonlinear term is computed directly in Fourier space (no pseudospectral method is used in the forcing scheme) so that dealiasing is not needed. Importantly, the velocity field corresponding to the truncated Euler dynamics mantains constant energy and helicity. Note that, with respect to previous works using Euler forcing [15, 8], our implementation allows to vary k_F arbitrarily, so that it is not restricted to $k_F = 1.5$.

The ABC forcing consists in adding in the Navier-Stokes equations an external volume force $\boldsymbol{F}_{\text{ABC}}$

corresponding to an Arnold-Beltrami-Childress flow (see *e.g.* [9])

$$\boldsymbol{F}_{\text{ABC}} = [B\cos(k_F\,y) + C\sin(k_F\,z)]\,\hat{\boldsymbol{i}} + [C\cos(k_F\,z) + A\sin(k_F\,x)]\,\hat{\boldsymbol{j}} + [A\cos(k_F\,x) + B\sin(k_F\,y)]\,\hat{\boldsymbol{k}}, \quad (8)$$

for a given chosen large scale wavenumber k_F. Since the force (8) is an eigenfunction of the curl operator with eigenvalue k_F, the ABC forcing injects helicity (in addition to energy) in the flow. For the ABC-forced runs described in section 3, $A = B = C$. For the sake of simplicity let the constants A, B and C be equal to 2. Then in Fourier space the expression (8) becomes

$$\begin{array}{rclcrcl}
\hat{\boldsymbol{F}}_{\text{ABC}} & = & [0 & \pm i & 1] & \text{if } \boldsymbol{k} & = & [\mp k_F & 0 & 0] \\
\hat{\boldsymbol{F}}_{\text{ABC}} & = & [1 & 0 & \pm i] & \text{if } \boldsymbol{k} & = & [0 & \mp k_F & 0] \\
\hat{\boldsymbol{F}}_{\text{ABC}} & = & [\pm i & 1 & 0] & \text{if } \boldsymbol{k} & = & [0 & 0 & \mp k_F] \\
\hat{\boldsymbol{F}}_{\text{ABC}} & = & [0 & 0 & 0] & \text{otherwise.} & & & & \\
\end{array}$$

No matter the value of k_F, only six modes are directly excited by the ABC force.

In terms of flow structure, the ABC forcing is very much like Taylor-Green vortices, but extended to three dimensions, so that it consists of permanent large scales rotors associated with a single wavelength. The Euler forcing has different properties, since the corresponding 3D large scale vortices evolve in time and interact in a manner closer to actual turbulent nonlinear dynamics, although in a non dissipative way. Moreover the forcing energy is distributed over a given range of large length scales.

2.1 Helical Euler forcing and helicity-free Euler forcing

In Euler-forced runs, Fourier coefficients for the forcing wavenumbers are initialized as a random solenoidal velocity field with energy spectrum proportional to

$$E(k) \propto k^{c_1}\,\mathrm{e}^{-(k/c_2)^2} \quad (9)$$

where c_1 and c_2 are constants linked to the energy spectrum peak wavenumber k_p. For the simulations reported in section 3, $k_p = k_F$. In order to control the helicity injection with the Euler forcing we implemented both a helicity-free and a helical modified initialization. The mean helicity can be computed as $\sum_{\boldsymbol{k}} h(\boldsymbol{k})$, where the helicity density $h(\boldsymbol{k}) = \hat{\boldsymbol{\omega}}(\boldsymbol{k}) \cdot \hat{\boldsymbol{u}}^*(\boldsymbol{k})$ can be re-expressed as a scalar triple product of the wavenumber and the real and imaginary parts of the velocity Fourier coefficient,

$$h(\boldsymbol{k}) = 2\,\boldsymbol{k} \cdot (\hat{\boldsymbol{u}}^R \times \hat{\boldsymbol{u}}^I). \quad (10)$$

In helical Euler-forced simulations, the initial values of the forced modes have been computed in order to obtain the maximal achievable helicity densities without changing the energy densities, *i.e.*

$$\hat{\boldsymbol{u}} = e(\boldsymbol{k})^{1/2}\,[\cos(\alpha)\,\boldsymbol{e}^{(1)} - \sin(\alpha)\,\boldsymbol{e}^{(2)}] + \mathbf{i}\,e(\boldsymbol{k})^{1/2}\,[\sin(\alpha)\,\boldsymbol{e}^{(1)} + \cos(\alpha)\,\boldsymbol{e}^{(2)}] \quad (11)$$

where α is a random angle and $e(\boldsymbol{k})$ is the energy density. In helicity-free Euler-forced simulations, even if the initial Eulerian velocity field described above already has nearly vanishing net helicity, we slightly modified the angles between the real and imaginary parts of all the forcing modes by the same quantity so that the net helicity is exactly zero, *i.e.* $\sum_{\boldsymbol{k}} h(\boldsymbol{k}) = 0$. Since the relative helicity in a helical forced

Run	Forcing	k_F	$k_{\max}\eta$	k_η	Re^λ	Re^L	$\mathcal{H}_{\text{rel}}$
1	hel.-free	5.5	1.20	142	82.4	239	-2.74E-3
2	helical	5.5	1.22	140	81.3	219	0.451
3	helical	5.5	1.19	143	81.7	210	0.617
4	ABC	5	1.38	123	81.9	216	0.643
5	helical	3.5	1.22	139	115	396	0.617
6	ABC	3	1.45	117	116	397	0.622
7	hel.-free	1.5	1.29	132	184	1119	2.19E-2

Table 1: Parameters used in the simulations. $k_{\max}$ is the maximum resolved wavenumber (after dealiasing), η is Kolmogorov length scale and $k_\eta = 1/\eta$. Re^λ and Re^L are the Taylor Reynolds number and the Reynolds number based on the longitudinal integral length scale L.

simulation depends on the prescribed energy spectrum, we used different shapes for the initial energy spectrum in order to achieve different relative helicities.

Note that, for instance, when net helicity is injected in a rapidly rotating (small Rossby number) turbulent flow, an inverse energy cascade takes place so that it can be impossible to reach a statistically stationary state. Unlike the ABC forcing, the Euler forcing is free from this drawback because of the conservative dynamics of the lowest modes $|\boldsymbol{k}| \leq k_F$.

3 Numerical results

We solved the incompressible Navier-Stokes equations in a periodic cube of side 2π with a classical Fourier pseudo-spectral approach. The code uses the 2/3-rule for dealiasing and a third-order Adams-Bashforth scheme for time marching. Since we are looking for non uniformity of statistics in a shell we have to introduce angular dependence in spectra [4, 11]. Angle-dependent energy spectra as well as modal decomposition of the energy spectra into poloidal and toroidal contributions were recently used in [16], permitting to study the scale-by-scale anisotropy of decaying (unforced) rotating homogeneous turbulence. Here, in non rotating forced homogeneous turbulence, we will study the anisotropy induced by Euler and ABC forcing on the generated turbulence by means of energy, helicity and polarization angle-dependent spectra with 512^3 resolution simulations. We considered variations with the angle θ between the vertical direction and the wavenumber, and divided evenly the interval $[0, \pi/2]$ in five sectors in order to compute five different spectra for every studied quantity. Of course the spectra have been normalized so that they collapse on the isotropic spectrum if anisotropy is absent.

Table 1 reports the parameters of the performed runs. In runs 1-4 we used $k_F = 5.5$ for Euler-forced simulations (which leads to 738 forcing modes in the Euler sphere) and $k_F = 5$ for the ABC-forced simulation, and we have made sure that the flow regimes, in terms of Reynolds numbers, are the same, so that a close comparison is permitted. Runs with helical forcing may have different relative helicities even if the other parameters are equal because the initial Eulerian velocity fields have different energy spectra. However, since we are interested in the statistically stationary solution (the so-called absolute equilibrium, see [2] for details), from now on we will refer to this solution for the spectrally truncated Euler equations. While in run 1 (helicity-free forcing) the largest wavenumber forcing modes hold roughly the same energy as the lowest ones, in run 2 (helical Euler forcing) the 48 largest wavenumber modes (over 738 forcing modes) hold 15 percent of the total energy. In run 3 (helical Euler forcing) the 48 largest wavenumber modes hold 92 percent of the kinetic energy in the Euler sphere so that the relative

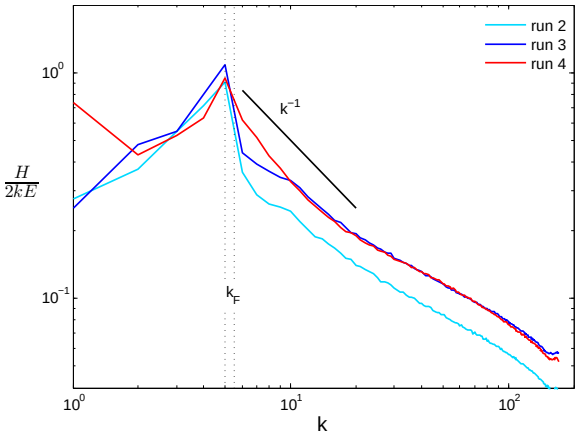

Figure 1: Relative helicity spectra for runs 2-4.

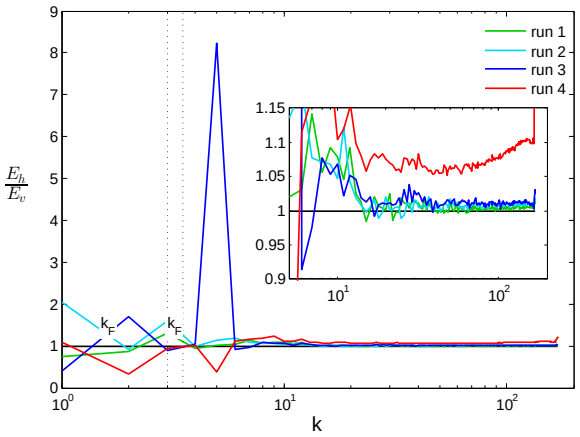

Figure 2: Ratio of horizontal to vertical sectors energy spectra for runs 1-4.

helicity is nearly equal to that of run 4 (ABC forcing). Runs 5 to 7 permit to investigate the effect of reducing the forcing wavenumber k_F.

In fig. 1 relative helicity spectra of runs 2-4 are plotted. A slope close to k^{-1} indicates that energy and helicity spectra scale with roughly the same power of k. The maximum value of relative helicity is nearly 1 and corresponds to the shell containing wavenumbers with modulus k_F for all of the three simulations. Fig. 2 shows the horizontal to vertical sector energy ratio for runs 1-4. Anisotropy develops at large scales in all runs, in particular for the ABC-forced run the horizontal sector energy is smaller than the vertical sector energy. This is consistent with the number of excited modes and the volumes of the sectors in Fourier space. In fact, the ABC force excites directly four modes in the horizontal sector and one mode in each vertical sector, but the volume of the horizontal sector is much greater than the volume of the vertical sector. Such a kind of computation is not suitable for helical Euler-forced simulations if some of the forcing modes in the largest shell have energy densities much greater than the other modes in the same shell. For example in run 3, none of the 48 most energetic modes is included in the vertical sector, while the horizontal sector contains 16 of them. Only in the ABC-forced simulation substantial anisotropy develops at small scales too. In particular the tendency is opposed to that at large scales, *i.e.* the horizontal sector energy is greater than that of the vertical sector. A more detailed description of the induced directional anisotropy can be achieved through angle-dependent energy spectra, which are shown in fig. 3. The Reynolds number is too low for an extended inertial range to exist in runs 1-4. However, the following runs are forced at lower wavenumbers so that the Reynolds number is higher. Since the departures from the isotropic energy spectrum are not clear on logarithmic scales, the directional anisotropy has to be investigated by plotting the spectra differences on a linear scale, see fig. 4. Large-scale directional anisotropy develops more or less in all runs. As expected, for run 4 (ABC forcing) the k_F-centered horizontal and vertical sectors hold more energy than the others, neverthless the opposite happens at small scales. A hint of small scale anisotropy is present in run 3 (helical Euler forcing, high relative helicity), but for run 4 it is definitely more important. Practically no small-scale directional anisotropy can be detected in runs 1 (helicity-free forcing) and 2 (helical Euler forcing, low relative helicity). Similar observations can be done for angular helicity spectra and helicity directional anisotropy of runs 2-4, see fig. 5 and 6. Finally, fig. 7 shows the angular dependence of the real part of polarization for runs 1-4. Again run 4 (ABC forcing) is the most anisotropic one and a hint of anisotropy is visible in run 3 (helical Euler forcing, high relative helicity) too. In every simulation, however, the

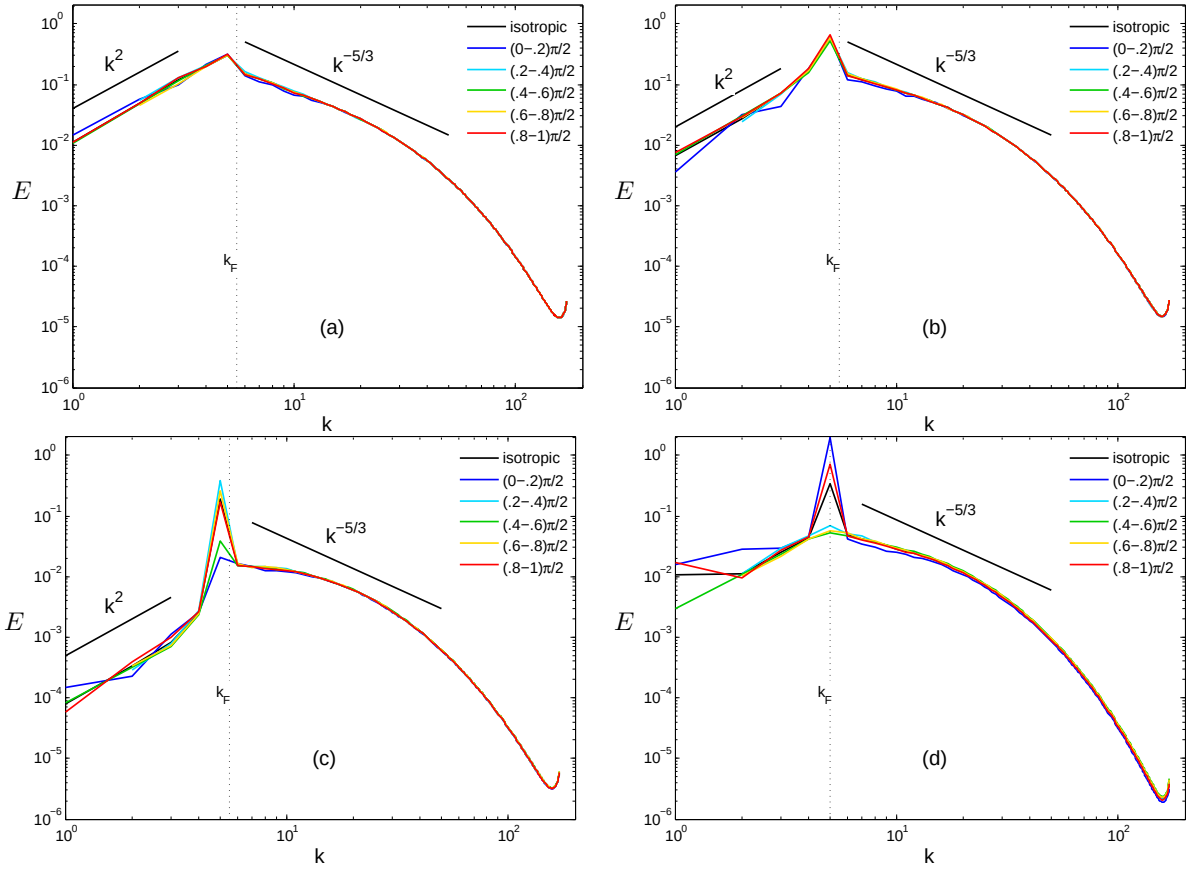

Figure 3: Angular energy spectra for: (a) run 1; (b) run 2; (c) run 3; (d) run 4.

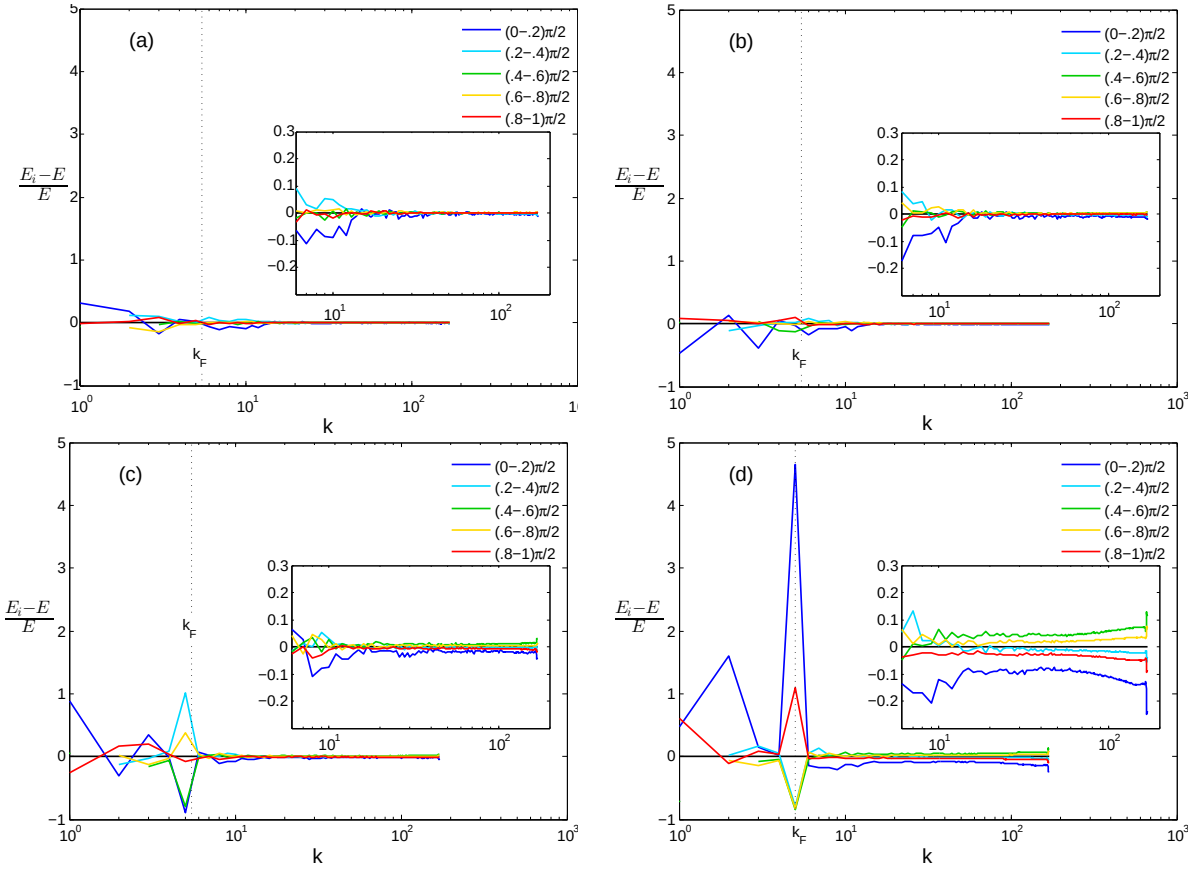

Figure 4: Directional anisotropy for: (a) run 1; (b) run 2; (c) run 3; (d) run 4.

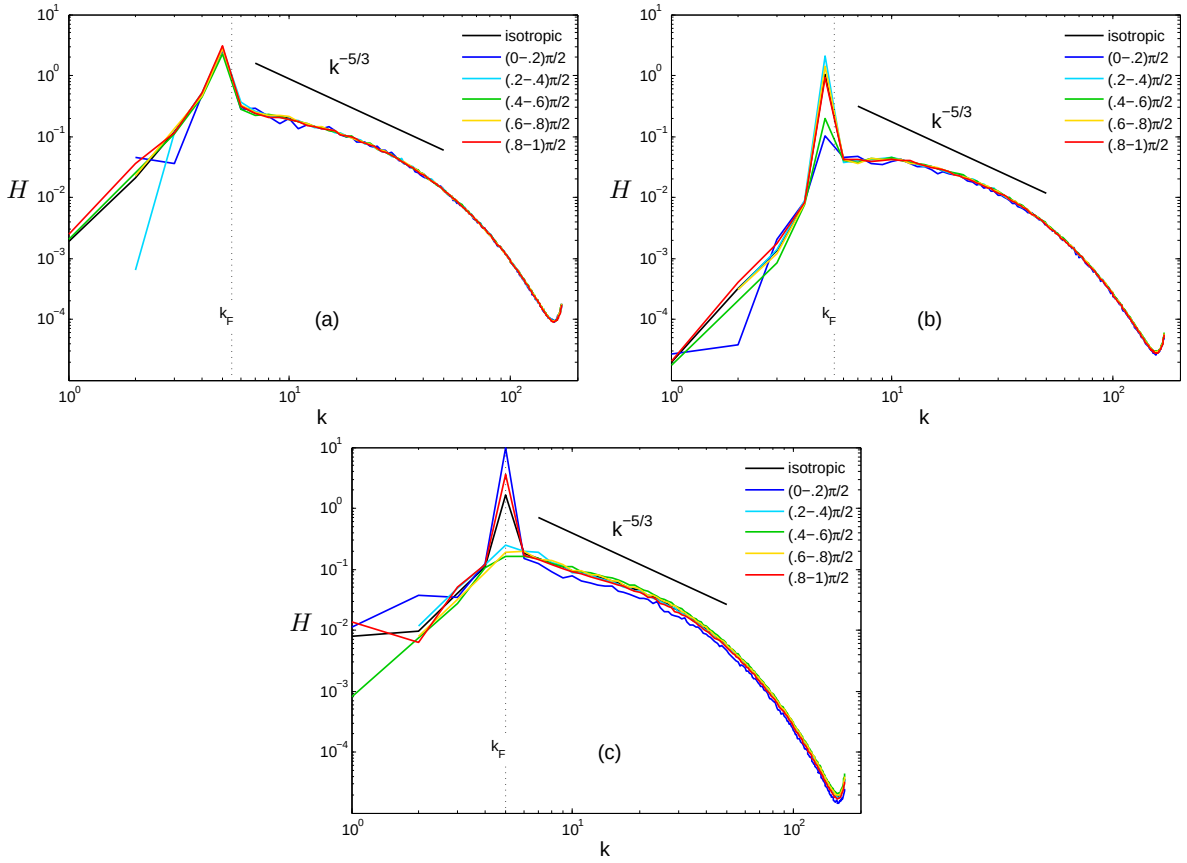

Figure 5: Angular helicity spectra for: (a) run 2; (b) run 3; (c) run 4.

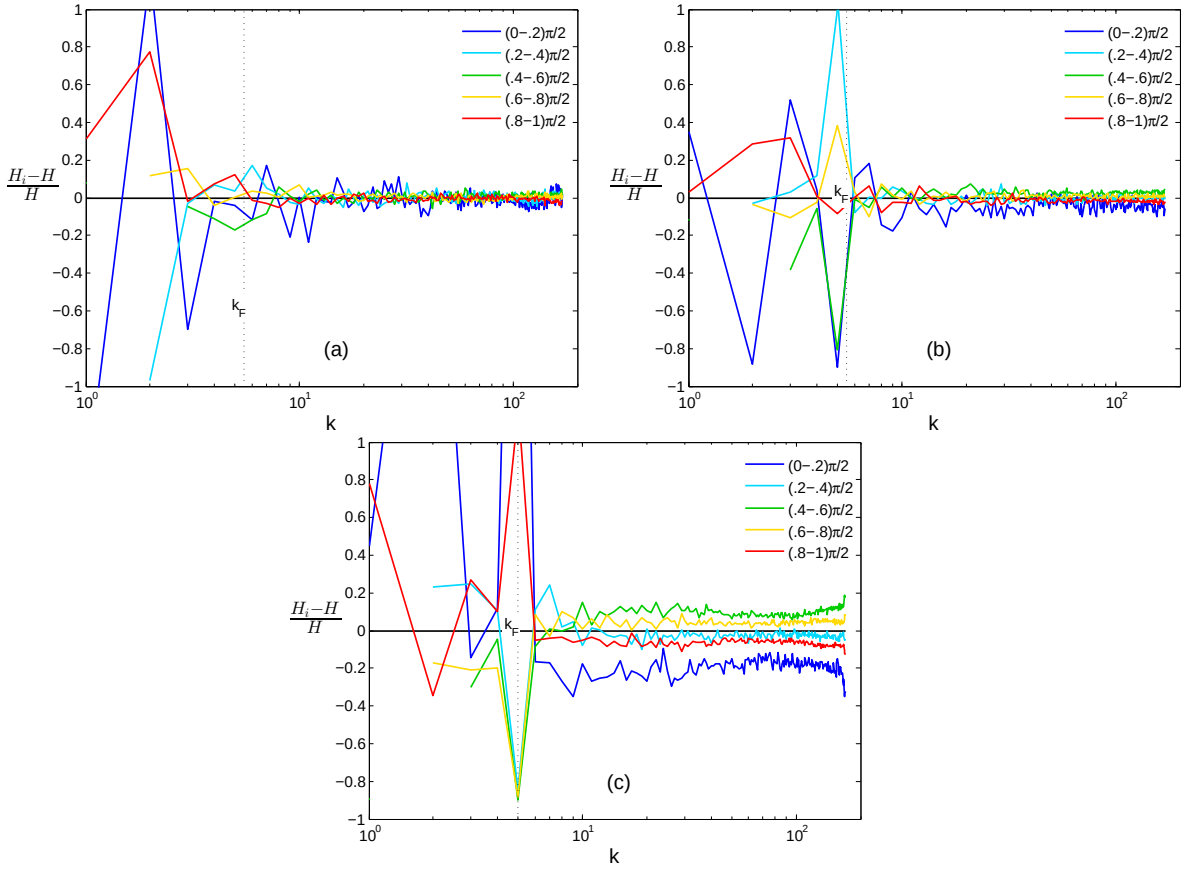

Figure 6: Helicity directional anisotropy for: (a) run 2; (b) run 3; (c) run 4.

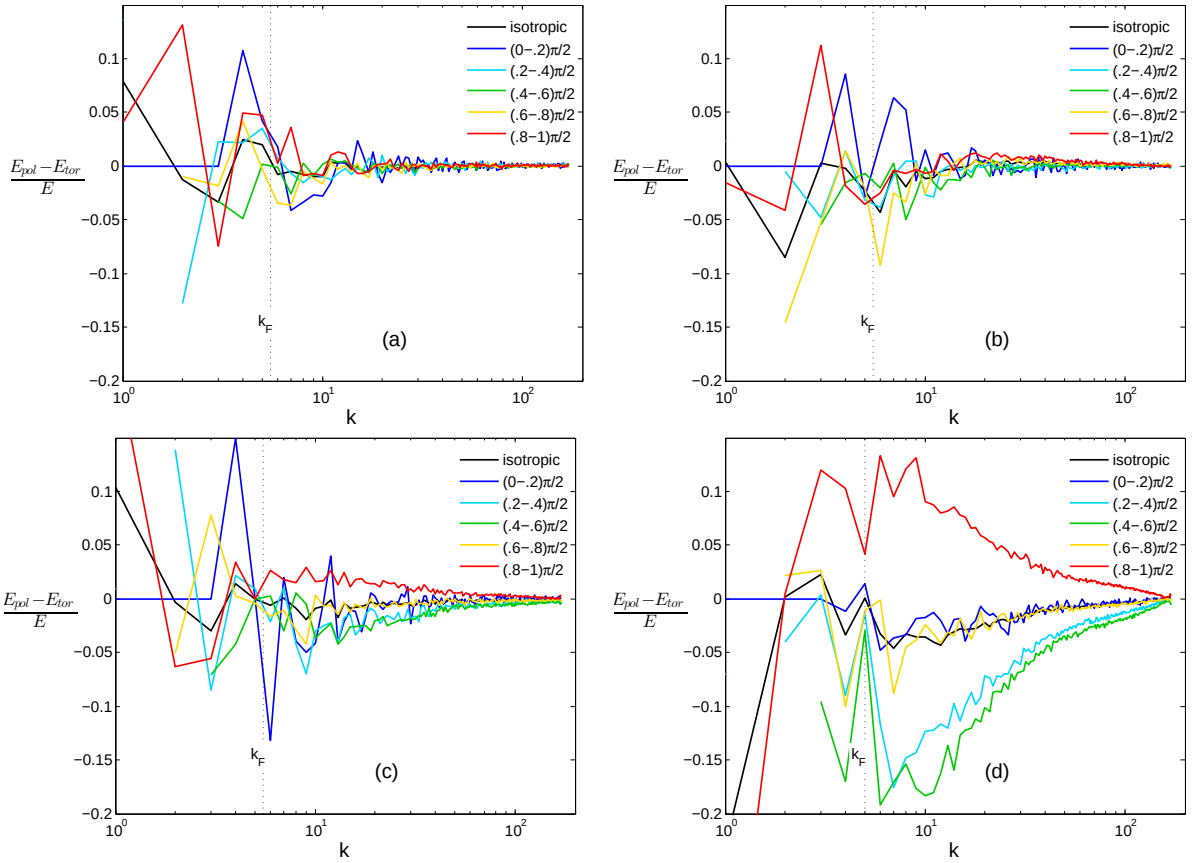

Figure 7: Real part of polarization for: (a) run 1; (b) run 2; (c) run 3; (d) run 4.

polarization directional anisotropy decreases with the wavenumber and vanishes at the smallest resolved scales.

Also if stronger anisotropy was observed in the ABC-forced simulation (run 4), an Euler-forced simulation can show a similar behaviour if k_F is low enough and the relative helicity is large enough. A helicity-free Euler-forced simulation cannot develop strong directional anisotropy. In fact, even the lowest possible forcing wavenumber, $k_F = 1.5$, leads to 18 forcing modes, which would have roughly the same energy densities in a helicity-free run. We performed a helical Euler-forced run with $k_F = 3.5$ and large relative helicity (run 5), an ABC-forced run with $k_F = 3$ (run 6) and a helicity-free Euler-forced run with $k_F = 1.5$ (run 7), see table 1. Similarly to run 3, in run 5 the 8 largest wavenumber modes (over 178 forcing modes) hold 81 percent of the Euler field energy. In fig. 8-13 some of the same statistics already plotted for runs 1-4 ($k_F = 5.5,\ 5$) are plotted for runs 5-7. For these figures, the helical Euler-forced run and the ABC-forced run have similar anisotropy levels (slightly lower than run 4, which was ABC-forced with $k_F = 5$), and directional anisotropy develops at all scales for run 5 too. The opposite tendencies between run 5 (helical Euler forcing) and run 6 (ABC forcing) in fig. 8-10 depend on the different orientation of wavenumbers corresponding to the most excited modes. By looking at fig. 4(d), 6(c), 8 and 9, that represent energy and helicity directional anisotropy for the ABC-forced runs with $k_F = 5$ and $k_F = 3$ and the helical Euler forced run with $k_F = 3.3$, one observes that the anisotropy for each angular sector is almost constant down to the smallest dissipative scales. Regarding run 7 (helicity-free forcing, $k_F = 1.5$), no anisotropy can be detected through the polarization angle-dependent spectrum, see fig. 13, and really small directional anisotropy arises at small scales, see fig. 12.

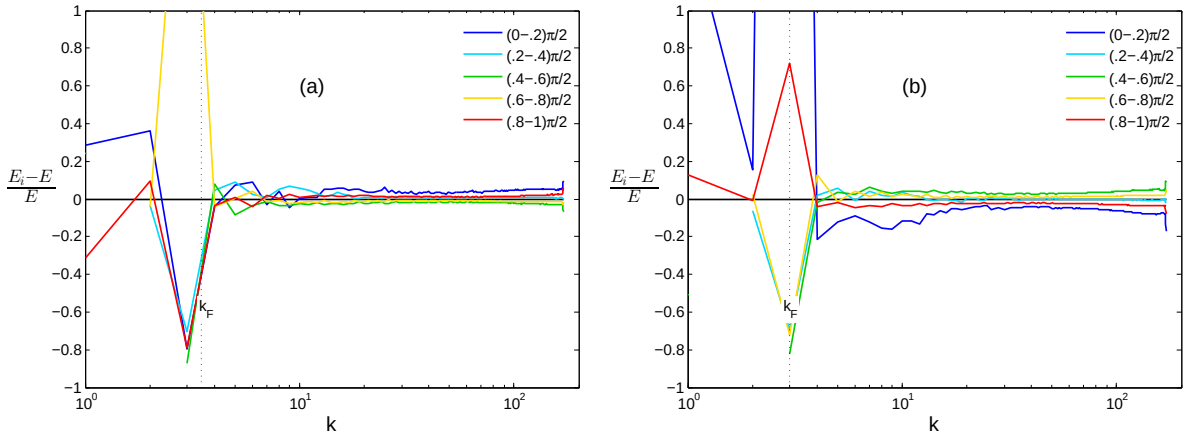

Figure 8: Directional anisotropy for: (a) run 5; (b) run 6.

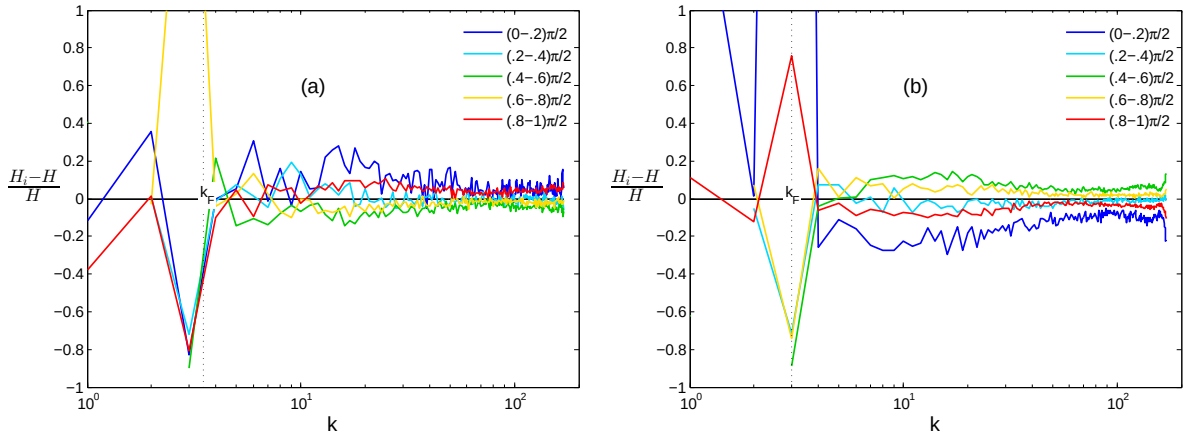

Figure 9: Helicity directional anisotropy for: (a) run 5; (b) run 6.

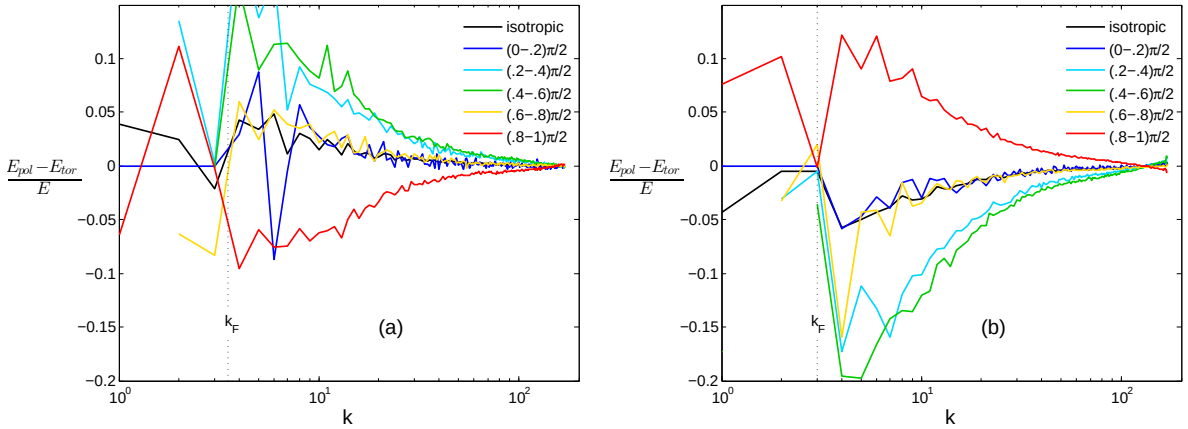

Figure 10: Real part of polarization for: (a) run 5; (b) run 6.

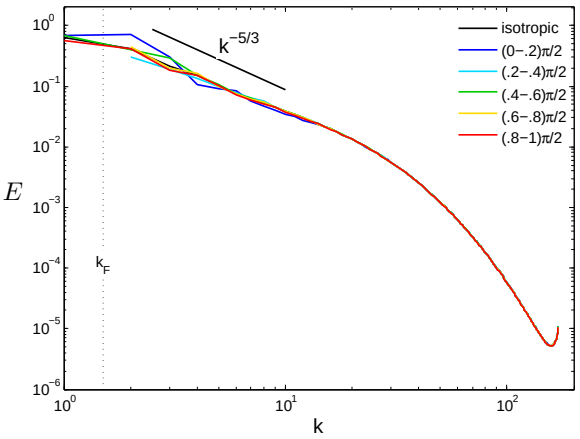

Figure 11: Angular energy spectra for run 7.

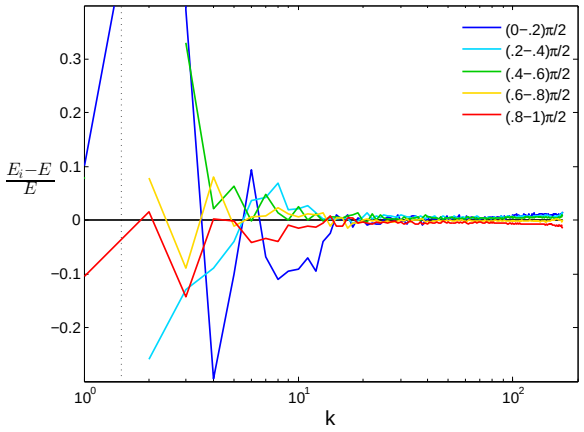

Figure 12: Directional anisotropy for run 7.

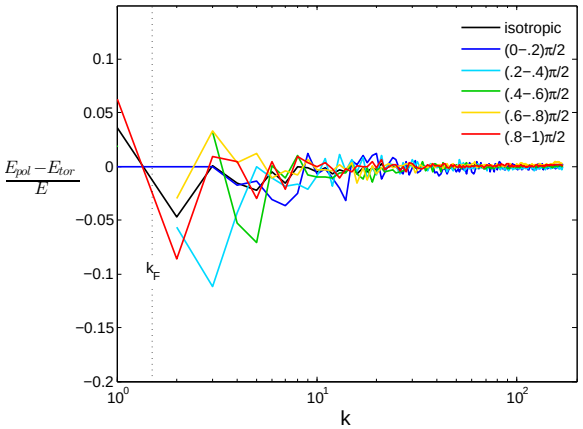

Figure 13: Real part of polarization for run 7.

4 Summary and conclusions

The effect of two large-scale spectral forcing methods, the Euler and the ABC forcing schemes, on refined two-point statistics, namely directional and polarization anisotropy, has been investigated through angle-dependent spectra. We showed that energy and helicity directional anisotropy can arise at all scales when the number of excited modes is too low or when few of the forcing modes hold much more energy than the others. Polarization anisotropy can develop too, but it gradually decreases as wavenumber increases so that small scales have no polarization anisotropy. Clearly, the ABC forcing scheme always affects the directional anisotropy because, regardless of k_F, only six modes are excited by the ABC force. Unlike ABC forcing, Euler forcing is not bound to exciting a rather limited number of modes. In fact, one can always set a large enough k_F, although it does not need to be very large. On the contrary, the requirement for the Euler forcing scheme to excite a low number of modes is setting up a low value for k_F, *i.e.* the Euler sphere in the Fourier space has to be small enough, and keeping the energy concentrated in the higher wavenumbers part of the spectrum, which can be achieved through a high value of the relative helicity.

This study is of strong importance when one will tackle the refined characterization of anisotropic forced turbulence submitted to external distorsions, such as rotating turbulence, stratified flows, or conducting fluid turbulence submitted to external magnetic field. All these contexts are important for modelling turbulent phenomena in geophysical or astrophysical flows.

References

[1] H. K. Moffatt. The degree of knottedness of tangled vortex lines. *J. Fluid Mech.* **35**: 117-129, 1969.

[2] R. H. Kraichnan. Helical turbulence and absolute equilibrium. *J. Fluid Mech.* **59**: 745-752, 1973.

[3] V. Eswaran, and S. B. Pope. An examination of forcing in direct numerical simulations of turbulence. *Comput. Fluids* **16**: 257-278, 1988.

[4] C. Cambon, and L. Jacquin. Spectral approach to non-isotropic turbulence subjected to rotation. *J. Fluid Mech.* **202**: 295-317, 1989.

[5] P. K. Yeung, and J. G. Brasseur. The response of isotropic turbulence to isotropic and anisotropic forcing at the large scales. *Phys. Fluids* **3**: 884, 1991.

[6] H. K. Moffatt. Helicity in laminar and turbulent flow. *Annu. Rev. Fluid Mech.* **24**: 281-312, 1992.

[7] N. P. Sullivan, S. Mahalingam, and R. M. Kerr. Deterministic forcing of homogeneous, isotropic turbulence. *Phys. Fluids* **6**: 1612-1614, 1994.

[8] A. Pumir. A numerical study of pressure fluctuations in three-dimensional, incompressible, homogeneous, isotropic turbulence *Phys. Fluids* **6**: 2071, 1994.

[9] S. Childress, and A. D. Gilbert. Stretch, twist, fold: the fast dynamo. *Springer-Verlag*, 1995.

[10] K. Alvelius. Random forcing of three-dimensional homogeneous turbulence. *Phys. Fluids* **11**: 1880-1889, 1999.

[11] F. S. Godeferd, and C. Staquet. Statistical modelling and direct numerical simulations of decaying stably-stratified turbulence. Part2. Large scales and small scales anisotropy. *J. Fluid Mech.* **486**: 115-150, 2003.

[12] P. Sagaut, and C. Cambon. Homogeneous Turbulence Dynamics. *Cambridge University Press*, 2008.

[13] P. D. Mininni, and A. Pouquet. Helicity cascades in rotating turbulence. *Phys. Rev. E* **79**: 026304, 2009.

[14] C. Lamriben, P. P. Cortet, and F. Moisy. Direct measurements of anisotropic energy transfers in a rotating turbulence experiment. *Phys. Rev. Lett.* **107**: 024503, 2011.

[15] A. Naso, and F. S. Godeferd. Statistics of the perceived velocity gradient tensor in a rotating turbulent flow. *New J. Phys.* **14**: 125002, 2012

[16] A. Delache, C. Cambon, and F. Godeferd. Scale by scale anisotropy in freely decaying rotating turbulence. *Phys. Fluids* **26**: 025104, 2014.